

Investigation of 3-D dynamic wind loads on lattice towers

Lianghao Zou[†] and Shuguo Liang^{‡*}

School of Civil and Building Engineering, Wuhan University, Wuhan, 430072, P.R. China

Q. S. Li^{‡†}

Department of Building and Construction, City University of Hong Kong, Hong Kong

Lin Zhao^{‡‡} and Yaojun Ge^{‡‡†}

Department of Bridge Engineering, Tongji University, Shanghai, 200092, P.R. China

(Received June 9, 2006, Accepted July 3, 2008)

Abstract. In this paper, the along-wind, across-wind as well as torsional dynamic wind loads on three kinds of lattice tower models are investigated using the base balance technique in a boundary layer wind tunnel. The models were specially designed, and their fundamental frequencies in the directions of the three principal axes are still in the frequency range of the spectra of wind loads on lattice towers. In order to clear contaminations to the spectra of wind loads induced by model resonance, the generalized force spectra of the first mode of the models in along-wind, across-wind and torsional directions were derived based on measured base moments of the models. The RMS generalized force coefficients are also obtained by removing the contributions of model resonance. Finally, the characteristics of the 3-D dynamic wind loads, especially those of the across-wind dynamic loads, on the three kinds of lattice towers are presented and discussed.

Keywords: lattice tower; wind load; wind tunnel test; generalized force spectrum.

1. Introduction

Wind loads, especially dynamic wind loads, on lattice towers are complex and difficult to determine. In recent years, full scale measurements and aero-elastic model tests in wind tunnels have indicated that wind-induced dynamic responses of lattice towers are not only in the along-wind direction, but also in the across-wind direction, and the oscillation amplitudes of displacements and accelerations of lattice towers in the across-wind direction could be as great as or even larger than

[†] Post Doctor Fellow

^{‡*} Professor, Corresponding author, E-mail: liangsg@public.wh.hb.cn

^{‡†} Associate Professor

^{‡‡} Lecturer

^{‡‡†} Professor

those in the along-wind direction (Glanville and Kwok 1995, Ballio, *et al.* 1992). For a certain case, this phenomenon is regarded as the strong-coupling which exists between the two horizontal principal axes of the lattice tower (Glanville and Kwok 1995). In the light of quasi-steady theory, several approaches, precise or simplified, have been developed to calculate along-wind dynamic responses of lattice towers under wind actions (Holmes 1994, 1996, Juhasova 1997, Yasui, *et al.* 1999). An experimental investigation on the wind forces on rectangular latticed communication towers with antennae was carried out by Carril, *et al.* and the mean and RMS wind forces on the tower models in both along-wind and across-wind directions were measured (2003). Models for the generation of wind velocity time-histories of transient tornado and microburst events and the resulting loading on a lattice tower were presented by Savory, *et al.* (2001). A full-scale field experiment on a 52 m tall steel lattice tower has been carried out by Harikrishna, *et al.* (1999) to measure wind characteristics and structural responses. The gust response factor for the base bending moment and top deflection have been evaluated using the measured structural responses and are compared with those obtained from several international wind codes using the measured wind velocities and the terrain roughness lengths. A spectral approach for computation of the along-wind response and the gust response factor of microwave lattice towers is presented by Venkateswarlu, *et al.* (1994). Full scale measurements of acceleration responses of a dynamically wind-sensitive lattice tower were conducted by Holmes, *et al.* (1992). Their measurements were compared with predictions of the along-wind responses using random vibration theory and available design information. Wyatt (1992) extended the classical stochastic dynamic analysis method of line-like structures to the case of a lattice tower with its axis inclined to the vertical, and conducted the dynamic gust response of this kind of inclined towers. A review of the literature reveals that extensive research has been conducted on the along-wind loads and responses for lattice tower structures, together with the across-wind loads and responses for several lattice towers. However, there is still a lack of a comprehensive study on the mechanism and prediction of the across-wind dynamic loads and responses of lattice towers.

To investigate dynamic loads on lattice towers induced by wind actions, this paper presents selected results of wind tunnel measurements of the along-wind, across-wind overturning moments and torsional moments of three kinds of typical lattice towers. The power spectral densities of the 3-D generalized wind loads and their RMS generalized force coefficients are further obtained by removing the contributions of model resonance.

2. Wind tunnel tests

Wind tunnel tests were carried out in the TJ-2 boundary layer wind tunnel in Tong Ji University, Shanghai, China. The test section of the wind tunnel is 3 m(width) \times 2 m(height) \times 15 m(length), and the turbulent wind field was simulated by the combination of spires and cubic elements upstream of the test section. The measured mean wind speeds and turbulence intensities at various heights over the test section are illustrated in Fig. 1, and the roughness length Z_0 at the test section was approximately 0.4cm. The longitudinal velocity spectrum of the simulated boundary layer wind flow at height 1m agrees with the von-Karman type spectrum well as shown in Fig. 2. The thickness of the simulated boundary layer was approximately 1.5 m, and the integral scales of the longitudinal component of along-wind turbulence L_u^x range from 30 to 50cm in the simulated boundary layer.

Three kinds of lattice tower models, which are a TV tower, an electrical transmission tower and a microwave communication tower, were considered in the wind tunnel study. Because dynamic wind loads on, and wind-induced vibrations of, an electrical transmission tower-line coupled system are

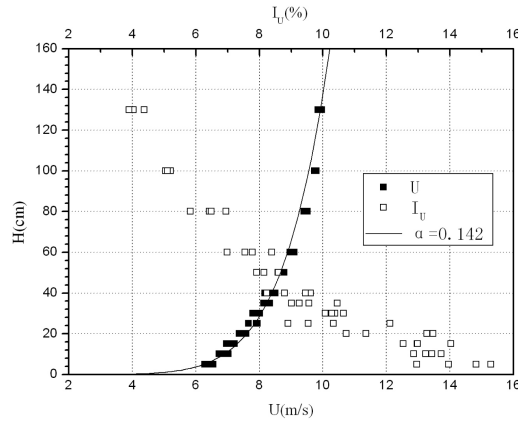


Fig. 1 The mean wind speed and the turbulent intensity profiles

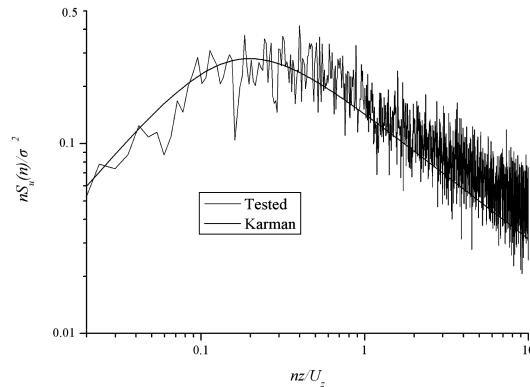


Fig. 2 The spectra of the wind speed

more complex problems which need further experimental and theoretical work, only dynamic wind loads on an electrical transmission tower without conductors and ground wires were considered in this study. Measurements of the dynamic wind loads on the lattice tower models were made by the base balance technique. The models of the lattice towers were made of copper. The geometric scale of the model for the TV tower is 1/100, and for the other two kinds of towers is 1/50. The basic members of the TV tower model are circular sheets and those of the other two tower models are angle sheets. The height of the TV tower model is 1.27 m, and each side of the hexagonal cross section at the bottom of the model is 0.13 m. The maximum width of the basic members of the TV tower model is 3mm, and the minimum is 1.2 mm. The diameter of glass tube simulating the elevator shaft at the center of the model is 25 mm. The height of the electrical transmission tower model is 0.97 m, and the section size at the bottom of the model is 0.179 m × 0.135 m. The maximum width of the basic members of the electrical transmission tower model is 2.8mm, and the minimum is 1.2 mm. The height of the microwave communication tower model is 0.97m, and the section size at the bottom of the model is 0.16 m × 0.16 m. The maximum width of the basic members of the communication tower model is 3.2 mm, and the minimum is 1.2 mm. Figs. 3-5 show the three models installed in the wind tunnel.



Fig. 3 The model of a TV tower

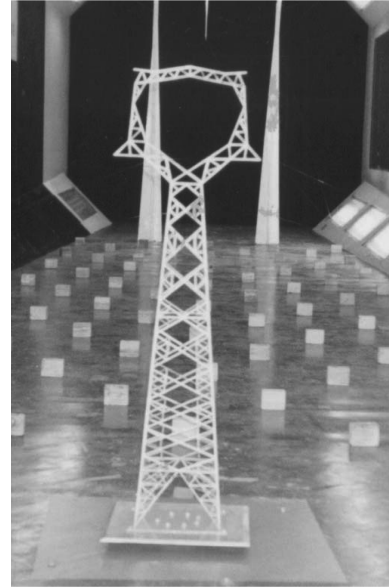


Fig. 4 The model of an electrical transmission tower

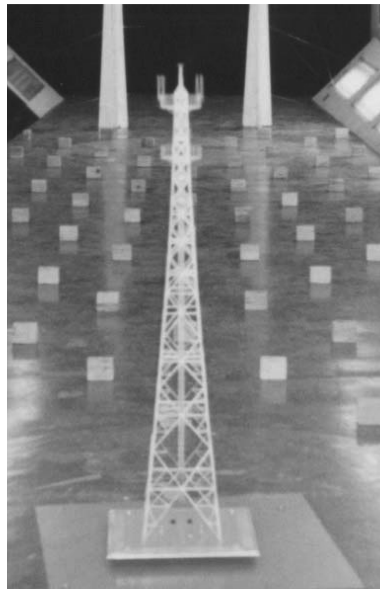


Fig. 5 The model of a micro-wave communication tower

Measurements of fluctuating wind forces were made with a carefully calibrated five-component, high frequency force balance. The sampling rates were 200 and 400 Hz for the models with geometric scale 1/50 and 1/100 respectively, and the sampling durations were 200 and 100 seconds for these two cases. The test wind speeds at height 1m were 10 m/s, and Reynolds numbers range from 800 to 2400 for different dimensions of the structural members of the electrical transmission

tower model and microwave communication tower model, and from 800 to 76000 for those of the TV tower model, in the wind tunnel tests.

3. Determination of the generalized force spectra

The models were specially designed, and their dynamic characteristics are limited by the nature of the materials of which the models were made; thus the fundamental frequencies in the directions of the three principal axes of the models are still in the effective frequency range of the spectra of wind loads on lattice towers. In order to clear contaminations from the spectra of wind loads induced by model resonance, the generalized force spectra of the first mode of the models in the along-wind, across-wind and torsional directions were derived based on measured base moments of the models.

The bending moment at the base of the model induced by fluctuating wind loads can be expressed as

$$M_F(t) = \int_0^H F(z, t)z dz \quad (1)$$

where $F(z, t)$ is a fluctuating wind load, whose mean equals zero, at height z of the models; H is the height of the model. When wind-induced vibration of the model takes place, the dynamic bending moment at the base of the model is the sum of the base bending moment induced by fluctuating wind loads and that induced by inertia force of the vibrating model, as well as that induced by damping force, and can be expressed as

$$M_0(t) = M_F(t) + M_I(t) + M_D(t) = \int_0^H F(z, t)z dz - \int_0^H m(z)\ddot{y}(z, t)z dz - \int_0^H C(z)\dot{y}(z, t)z dz \quad (2)$$

where $m(z)$ and $C(z)$ = the mass and damping coefficient of the model at height z respectively. $\ddot{y}(z, t)$, $\dot{y}(z, t)$ = acceleration and velocity of the model at height z respectively. According to the mode super-position method, we have

$$y(z, t) = \sum_{i=1}^{\infty} \phi_i(z)q_i(t) \quad (3)$$

$$\dot{y}(z, t) = \sum_{i=1}^{\infty} \phi_i(z)\dot{q}_i(t) \quad (4)$$

$$\ddot{y}(z, t) = \sum_{i=1}^{\infty} \phi_i(z)\ddot{q}_i(t) \quad (5)$$

Where $\phi_i(z)$ is the i -th mode shape at height z in the lateral direction, and $q_i(t)$, $\dot{q}_i(t)$ and $\ddot{q}_i(t)$ are the generalized displacement, velocity and acceleration of the i -th mode respectively.

Substituting Eq. (4) and Eq. (5) into Eq. (2), we obtain:

$$M_0(t) = H \int_0^H F(z, t) \frac{z}{H} dz - H \int_0^H m(z) \sum_{i=1}^{\infty} \phi_i(z) \ddot{q}_i(t) \frac{z}{H} dz - H \int_0^H C(z) \sum_{i=1}^{\infty} \phi_i(z) \dot{q}_i(t) \frac{z}{H} dz \quad (6)$$

Assuming that the fundamental mode shape of the model in lateral directions is linear, expressed by

$$\phi_1(z) = \frac{z}{H} \quad (7)$$

and utilizing orthogonality property of vibration modes, we can deduce

$$\frac{M_0(t)}{H} = \int_0^H F(z, t) \phi_1(z) dz - \ddot{q}_1 M_1^* - \dot{q}_1 C_1^* \quad (8)$$

in which M_1^* and C_1^* the generalized mass and damping coefficient of the first mode respectively. Let $S_M(\omega)$ be the power spectrum of the bending moment at the base of the model, $M_0(t)$, and $S_{F_1}^*(\omega)$ be the generalized wind force spectrum of the first mode. The generalized velocity response spectrum and acceleration response spectrum of the first mode can be expressed as

$$S_{\dot{q}_1}(\omega) = |H_1(i\omega)|^2 \omega^2 S_{F_1}^*(\omega) / M_1^{*2} \quad (9)$$

and

$$S_{\ddot{q}_1}(\omega) = |H_1(i\omega)|^2 \omega^4 S_{F_1}^*(\omega) / M_1^{*2} \quad (10)$$

respectively. Conducting a Fourier transform on the autocorrelation function of Eq. (8), and neglecting cross terms, which are zero or very small (Wang and Liang 2004), we obtain

$$\frac{S_M(\omega)}{H^2} \approx S_{F_1}^*(\omega) + \frac{|H_1(i\omega)|^2 \omega^4 S_{F_1}^*(\omega)}{M_1^{*2}} M_1^{*2} + \frac{|H_1(i\omega)|^2 \omega^2 S_{F_1}^*(\omega)}{M_1^{*2}} C_1^{*2} \quad (11)$$

Therefore, the generalized wind force spectrum of the first mode can be derived as

$$S_{F_1}^*(\omega) = \frac{S_M(\omega)}{H^2 (1 + |H_1(i\omega)|^2 \omega^4 + |H_1(i\omega)|^2 \omega^2 4 \xi_1^2 \omega_1^2)} \quad (12)$$

where, ξ_1 and ω_1 = the damping ratio and natural circular frequency of the first mode of the model in the direction of a horizontal principal axis respectively.

Similarly, the torque at the base of the model induced by fluctuating wind loads can be expressed as

$$N_F(t) = \int_0^H N(z, t) dz \quad (13)$$

where $N(z, t)$ is wind-induced fluctuating torque, whose mean equals zero, at height z of the model. When wind-induced torsional vibration of the model takes place, the dynamic torque at the base of the model is the sum of the base torque induced by fluctuating wind loads and that induced by moment of inertia of the vibrating model in the torsional direction as well as that induced by the damping force, and can be expressed as

$$N_0(t) = N_F(t) + N_I(t) + N_D(t) = \int_0^H N(z, t) dz - \int_0^H J(z, t) \ddot{\theta}(z, t) dz - \int_0^H C_T(z) \dot{\theta}(z, t) dz \quad (14)$$

where $J(z)$ and $C_T(z)$ = the moment of inertia and torsional damping coefficient of the model at

height z respectively. $\dot{\theta}(z, t)$ and $\ddot{\theta}(z, t)$ = the angular velocity and angular acceleration of the model at height z respectively. According to the mode super-position method, we have

$$\theta(z, t) = \sum_{i=1}^{\infty} \varphi_i(z) \gamma_i(t) \quad (15)$$

$$\dot{\theta}(z, t) = \sum_{i=1}^{\infty} \varphi_i(z) \dot{\gamma}_i(t) \quad (16)$$

$$\ddot{\theta}(z, t) = \sum_{i=1}^{\infty} \varphi_i(z) \ddot{\gamma}_i(t) \quad (17)$$

Where $\varphi_i(z)$ = the i -th mode shape at height z in torsional direction, and $\gamma_i(t)$, $\dot{\gamma}_i(t)$ and $\ddot{\gamma}_i(t)$ = the generalized displacement, velocity and acceleration of the i -th mode respectively.

Substituting Eq. (16) and Eq. (17) into Eq. (14), we obtain

$$N_0(t) = \int_0^H N(z, t) dz - \int_0^H J(z) \sum_{i=1}^{\infty} \varphi_i(z) \ddot{\gamma}_i(t) dz - \int_0^H C_T(z) \sum_{i=1}^{\infty} \varphi_i(z) \dot{\gamma}_i(t) dz \quad (18)$$

Assuming the fundamental torsion mode shape φ_1 is a constant, and by defining a mode shape modulation coefficient $L = 1/\varphi_1$, Eq. (18) becomes

$$N_0(t) = L \int_0^H N(z, t) \varphi_1 dz - L \int_0^H J(z) \sum_{i=1}^{\infty} \varphi_i(z) \ddot{\gamma}_i(t) \varphi_1 dz - L \int_0^H C_T(z) \sum_{i=1}^{\infty} \varphi_i(z) \dot{\gamma}_i(t) \varphi_1 dz \quad (19)$$

Utilizing the orthogonality property of vibration modes, we obtain

$$\frac{N_0(t)}{L} = \int_0^H N(z, t) \varphi_1 dz - \ddot{\gamma}_1(t) J_1^* - \dot{\gamma}_1(t) C_{T1}^* \quad (20)$$

in which J_1^* and C_{T1}^* = the generalized moment of inertia and torsional damping coefficient of the first mode of the model respectively. Let $S_T(\omega)$ be the power spectrum of the torque at the base of the model, $N_0(t)$, and $S_{N_1}^*(\omega)$ be the generalized torque spectrum of the first mode. The generalized angular velocity and acceleration response spectra of the first mode can be expressed as

$$S_{\dot{\gamma}_1}(\omega) = |H_{T1}(i\omega)|^2 \omega^2 S_{N_1}^*(\omega) / J_1^{*2} \quad (21)$$

and

$$S_{\ddot{\gamma}_1}(\omega) = |H_{T1}(i\omega)|^2 \omega^4 S_{N_1}^*(\omega) / J_1^{*2} \quad (22)$$

respectively. Conducting a Fourier transform on the autocorrelation function of Eq. (20), and neglecting cross terms, which are zero or very small, we obtain

$$\frac{S_T(\omega)}{L^2} \approx S_{N_1}^*(\omega) + \frac{|H_{T1}(i\omega)|^2 \omega^4 S_{N_1}^*(\omega)}{J_1^{*2}} J_1^{*2} + \frac{|H_{T1}(i\omega)|^2 \omega^2 S_{N_1}^*(\omega)}{J_1^{*2}} C_{T1}^{*2} \quad (23)$$

Therefore, the generalized torque spectrum of the first mode can be derived as

$$S_{N_1}^*(\omega) = \frac{S_T(\omega)}{L^2(1 + |H_{T1}(i\omega)|^2 \omega^4 + |H_{T1}(i\omega)|^2 \omega^2 4 \xi_{T1}^2 \omega_{T1}^2)} \quad (24)$$

where, ξ_{T1} and ω_{T1} = the damping ratio and natural circular frequency of the first mode of the model in the torsional direction, respectively.

4. The generalized force spectra and RMS coefficients

By removing the contributions of model resonance, the power spectral densities of 3-D generalized wind loads and their RMS generalized force coefficients can be obtained for different angles of approaching flow through a data processing procedure.

4.1. The power spectra of 3-D generalized wind loads of the first mode

4.1.1. The electrical transmission tower model

Five angles of approaching wind were considered in the wind tunnel tests for the electricity transmission tower. The normalized generalized force spectra of the first mode of the model in the X-axial, Y-axial and torsional directions for angles 0° , 45° and 90° are illustrated in Figs. 6, 7 and 8 respectively, where in the reduced frequency nB/V_H , B is the width of the bottom section of the model, and V_H is the mean wind speed at the top of the model. The average solidity ratio of the model in the X- axial direction is 0.135, and in the Y- axial direction is 0.150.

The distinctive characteristics of the power spectra of along-wind, across-wind and torsional generalized wind loads can be observed from Figs. 6, 7 and 8 respectively. The peaks of the spectral density of the along-wind generalized loads are located at the very lowest reduced frequencies, and gradually decline as the reduced frequency increases, which can be seen in Figs. 6 and 8. The peaks of

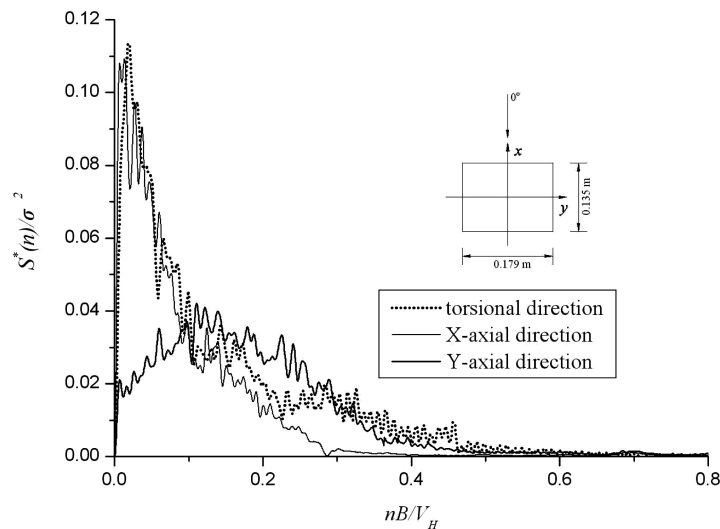


Fig. 6 The generalized force spectra of the transmission tower model for angle 0°

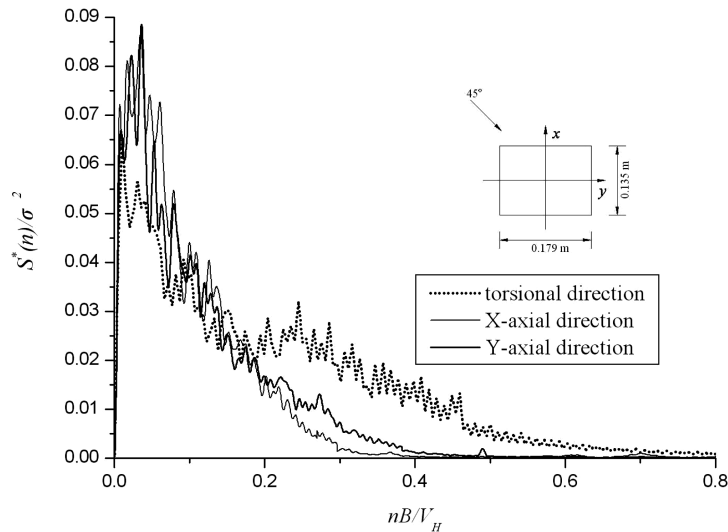


Fig. 7 The generalized force spectra of the transmission tower model for angle 45°

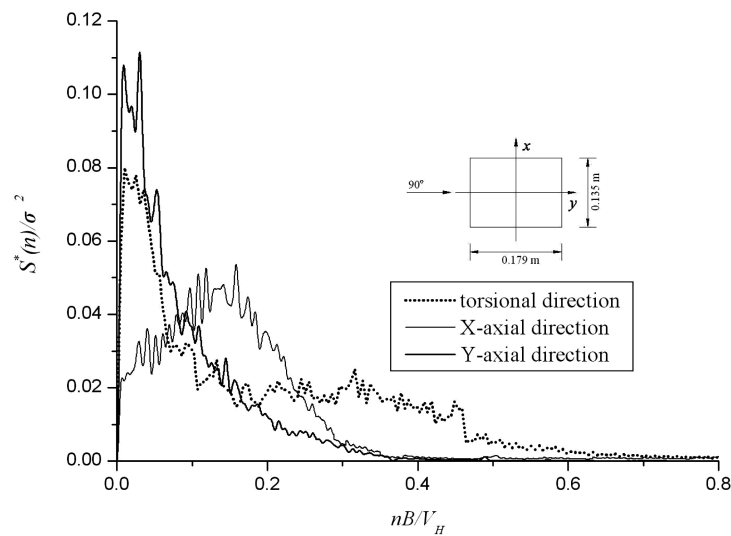


Fig. 8 The generalized force spectra of the transmission tower model for angle 90°

the spectral density of across-wind generalized loads are located at a relatively higher reduced frequency range compared with those of the along-wind generalized loads, and the bandwidths of the peaks are rather wider as shown in Figs. 6 and 8. The power spectra of torsional generalized wind loads have typical wide-band characteristics, and their peaks are also at the very lowest reduced frequencies as shown in Figs. 6, 7 and 8. When the angle of the approaching flow is just between the two horizontal principal axes, the magnitude and distribution of the power spectra of generalized wind loads in the X-axial and Y-axial directions are almost the same as shown in Fig. 7, and they are similar to those of the generalized force spectra in the along-wind direction as shown in Figs. 6 and 8.

4.1.2. The TV tower model

There were five test angles of incident wind in the wind tunnel test for the TV tower model. The generalized force spectra of the first mode of the model in the X-axial, Y-axial and torsional directions for angles of 0° , 45° and 90° are illustrated in Figs. 9, 10 and 11 respectively. The average solidity ratio of the model in the X- axial direction is 0.395, and in the Y- axial direction is 0.430.

The spectral densities of the generalized wind loads on the TV tower model, as shown in Figs. 9-11, have similar characteristics to those of the electrical transmission tower model. The TV tower is actually not a pure lattice tower. The cross sections of the basic members of the tower structure are

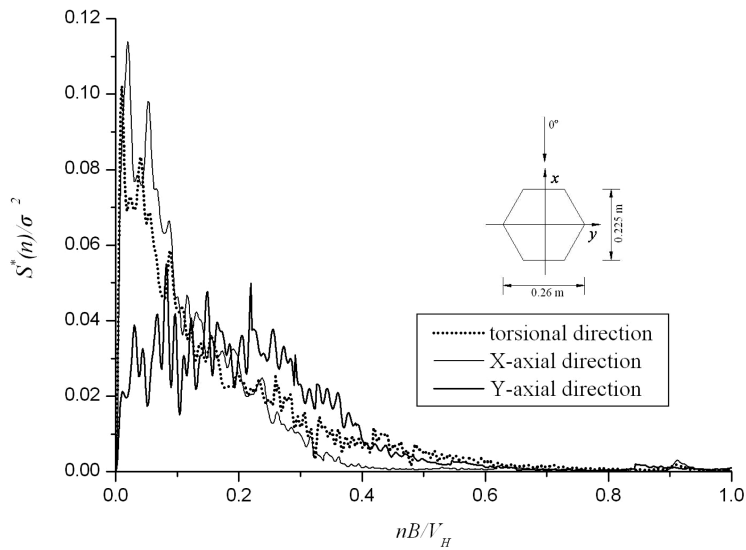


Fig. 9 The generalized force spectra of the TV tower model for angle 0°

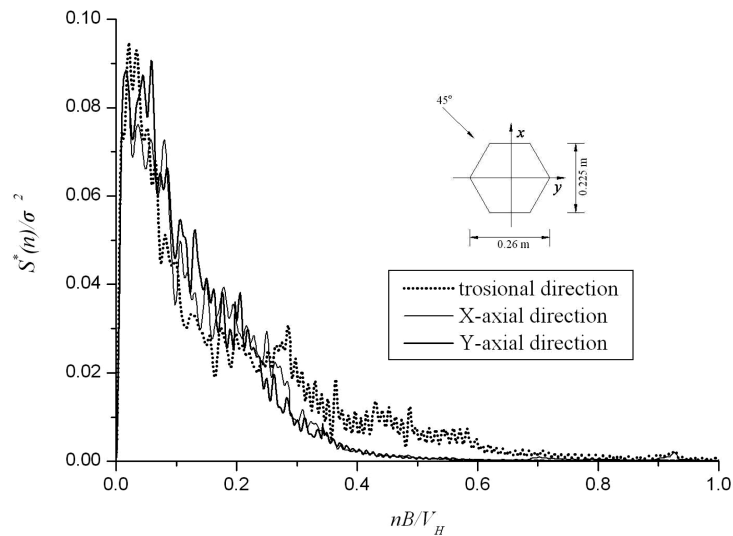


Fig. 10 The generalized force spectra of the TV tower model for angle 45°

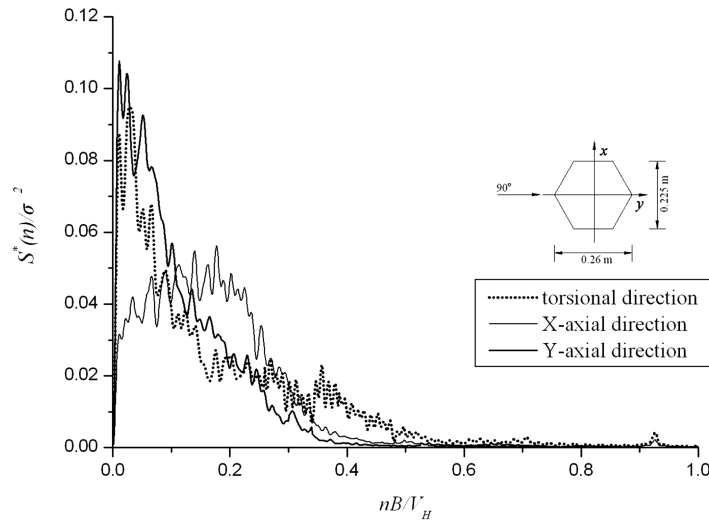


Fig. 11 The generalized force spectra of the TV tower model for angle 90°

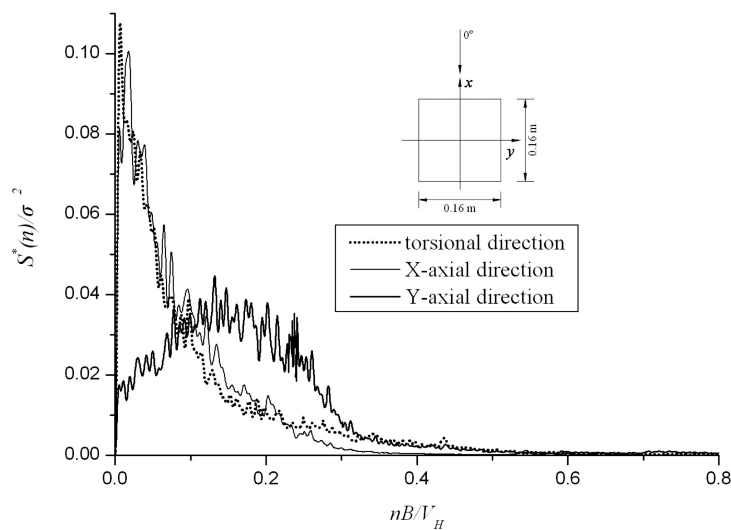


Fig. 12 The generalized force spectra of the communication tower model for angle 0°

circular, and the cross section of its mast is square; moreover, the sight-view part of the tower is a relatively huge solid of revolution. Therefore, the wind-induced pressures have different characteristics at different parts of the tower because of their distinctive flow fields. Under the influences of above-mentioned factors, the curves of the spectral densities of the generalized wind loads on the TV tower model become partially irregular, though their rough shapes seem to be similar to those of the electrical transmission tower.

4.1.3 The micro-wave communication tower model

There were five test angles of approaching wind for the microwave communication tower model.

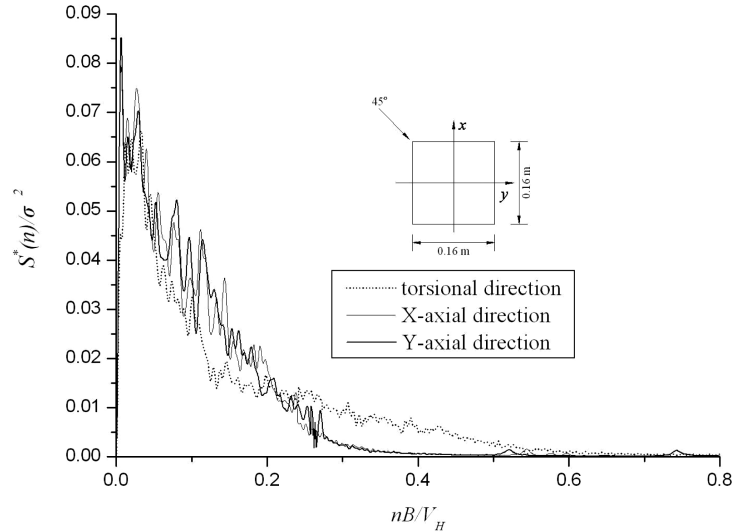


Fig. 13 The generalized force spectra of the communication tower model for angle 45°

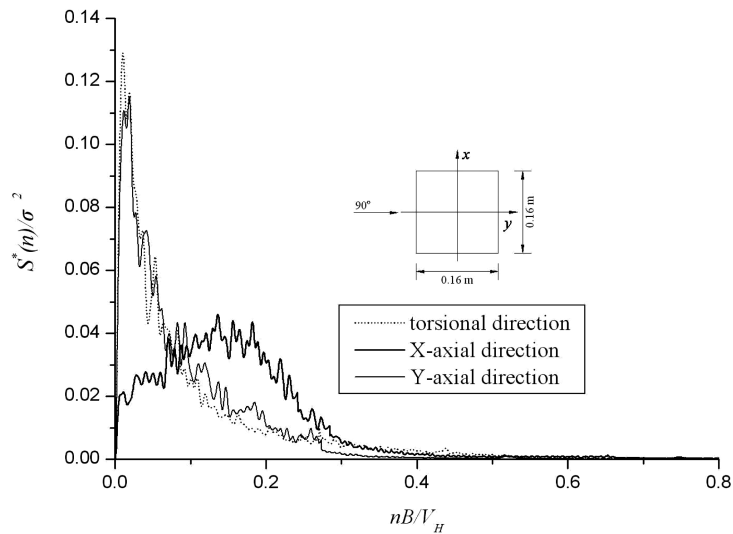


Fig. 14 The generalized force spectra of the communication tower model for angle 90°

The generalized force spectra of the first mode of the model in the X-axial, Y-axial and torsional directions for angles of 0° , 45° and 90° are illustrated in Figs. 12, 13 and 14 respectively. The average solidity ratio of the model in the X- axial direction is 0.152, and in the Y- axial direction is 0.158.

The characteristics of the spectral densities of the generalized wind loads on the model of the micro-wave communication tower are also similar to those of the electrical transmission tower. Because of the general dual-axial symmetry of the cross section, the curves of the spectral densities of the generalized 3-D wind loads on the model of the micro-wave communication tower for the angle of 90° are almost the same as those for angle of 0° .

4.2. The RMS generalized force coefficients

To evaluate the magnitudes of the fluctuating 3-D wind loads on the three models, the RMS generalized force coefficients in the X-axial, Y-axial and torsional directions are also obtained based on the measured data. The formulae for determining the RMS generalized force coefficients in X-axial, Y-axial and torsional directions are as follows:

$$C_X = \frac{\sigma_{F_X^*}}{\rho V_H^2 AR/2} \quad (25)$$

$$C_Y = \frac{\sigma_{F_Y^*}}{\rho V_H^2 AR/2} \quad (26)$$

$$C_T = \frac{\sigma_{F_T^*}}{\rho V_H^2 ABR/2} \quad (27)$$

where, $\sigma_{F_X^*}$, $\sigma_{F_Y^*}$ and $\sigma_{F_T^*}$ are the RMS of the generalized wind loads in the X-axial, Y-axial and torsional direction respectively, which are equal to the square root of the area of the spectral densities of generalized wind loads in corresponding direction; A is the contour area of the lattice tower in the X-axial direction; R is the solidity ratio of area A ; B is the width of the lattice tower; ρ is the air mass density; V_H is the mean wind speed at the height of the lattice tower.

Figs. 15, 16 and 17 show that the RMS generalized force coefficients in the along-wind direction are much greater than those in across-wind direction, and the RMS generalized force coefficients in the torsional direction are the smallest, and are almost constant as the angle of the approach wind changes. Meanwhile, the RMS generalized force coefficients of the TV tower are much less than those of the electrical transmission tower and micro-wave communication tower because of its larger solidity ratio and circular cross section of the basic lattice members.

5. Analysis and discussion

The average wind loads on, as well as the drag force coefficients of, the lattice tower models in the wind tunnel tests were also investigated to examine the accuracy of the base force measurements presented in this paper. Taking the communication tower model as an example, the drag force coefficient of the model can be evaluated by the following two formulae:

$$\mu_{sM} = \frac{\bar{M}}{\int_0^H \frac{1}{2} \rho V_H^2 \left(\frac{z}{H}\right)^{2\alpha} R(z) B(z) z dz} \quad (28)$$

$$\mu_{sV} = \frac{\bar{Q}}{\int_0^H \frac{1}{2} \rho V_H^2 \left(\frac{z}{H}\right)^{2\alpha} R(z) B(z) dz} \quad (29)$$

where, $R(z)$ is the solidity ratio at height z ; H is the height of the model; V_H is the mean wind speed at the height of the model; α is the exponent of the power law in the mean wind speed profile; $B(z)$

is the width of the model at height z ; \bar{M} and \bar{Q} are the measured mean base bending moment and shear force in the along wind direction; μ_{sM} and μ_{sV} are the drag force coefficients acquired from the measured mean base bending moment and shear force respectively.

The drag force coefficients of the communication tower model in the wind tunnel tests and the corresponding values with the same solidity ratios in the European and ASCE Standards(2004, 2002) are listed in Table 1. The comparison of the drag force coefficients between the experimental results and those estimated by two well-known wind loading standards indicates the difference

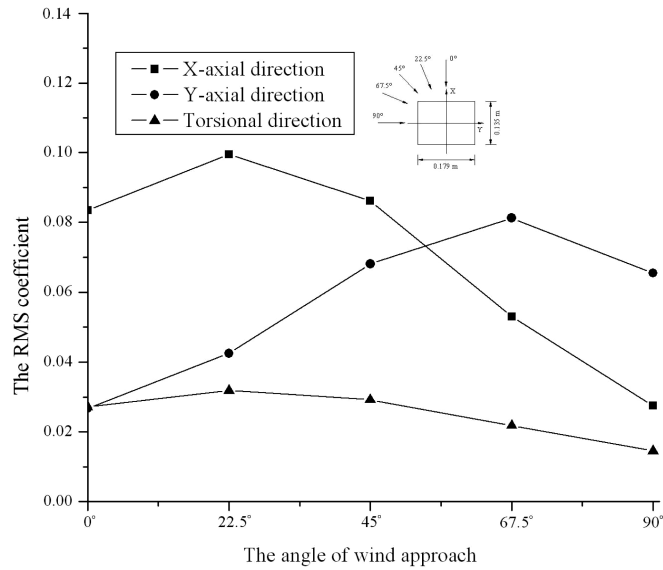


Fig. 15 The RMS generalized force coefficients for the transmission tower

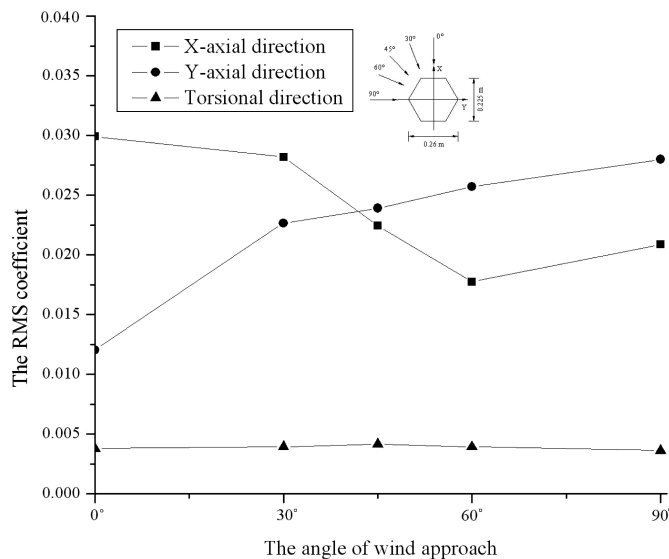


Fig. 16 The RMS generalized force coefficients for the TV tower

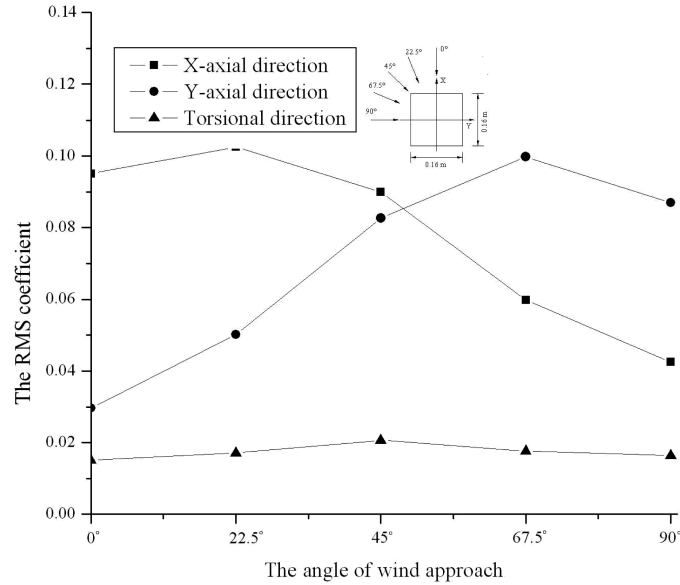


Fig. 17 The RMS generalized force coefficients for the communication tower

Table 1 Comparison of the drag force coefficients between experimental results and those estimated by international standards

Lattice structure		The communication tower	
Solidity ratio in X- axial direction		0.152	
Drag force coefficients	Experimental results	μ_{sM}	3.08
		μ_{sV}	3.13
	European standard		3.05
	ASCE		3.196

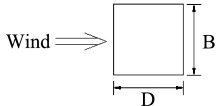
between them are fairly small, and the measured base bending moments and shear forces in the wind tunnel tests should be reliable and applicable.

The measured along-wind and across-wind forces of the lattice tower models in the wind tunnel tests also can be compared with the previous experimental results obtained by Carril *et al.* (2003). Besides the drag force coefficients of the communication tower model in the wind tunnel tests listed in Table 1, the RMS along-wind and across-wind force coefficients of which can be calculated as follows:

$$\mu_{\sigma M} = \frac{\sigma_M}{\int_0^H \frac{1}{2} \rho V_H^2 \left(\frac{z}{H}\right)^{2\alpha} R(z) B(z) z dz} \tag{30}$$

where, σ_M is the RMS of the base bending moment in the along-wind or across-wind direction, in which, the influence induced by the model resonance was cleared; $\mu_{\sigma M}$ is the RMS along-wind or across-wind force coefficient acquired from the measured RMS base bending moment in the along-wind or across-wind direction. Then, the drag force coefficients, as well as the RMS along-wind and across-wind force coefficients, of the communication tower model in the wind tunnel tests and

Table 2 Comparison of the force coefficients between experimental results of the two lattice models in turbulent flow

Lattice structures	The communication tower model in this paper				The section model 3 in Carril, <i>et al.</i> (2003)		
	$D/B = 1/1$				$D/B=3/1$		
	Re	Solidity ratio	Results		Re	Solidity ratio	Results
	Drag force coefficients	800~2400	0.152	μ_{sM}	3.08	4009	0.162
μ_{sV}				3.13	5010	3.18	
					6424	3.11	
RMS along-wind force coefficients	800~2400	0.152	0°	0.283	4009	0.162	0.127
			90°	0.273	5010		0.127
					6424		0.126
RMS across-wind force coefficients	800~2400	0.152	0°	0.093	4009	0.162	0.042
			90°	0.119	5010		0.043
					6424		0.049

Note: The azimuths in this table are specified in Fig. 17.

the corresponding wind tunnel data of the model 3, which were presented by Carril, *et al.* (2003), are listed in Table 2 to compare the magnitudes of average and fluctuating wind forces of the two rectangular lattice tower models under similar, but not identical, experimental conditions.

The data in Table 2 indicate that the differences between the drag force coefficients of the two models are very small, for the solidity ratios of the two models are close to each other. In contrast, the differences between the RMS along-wind and across-wind force coefficients of the two models are rather large, and the RMS along-wind and across-wind force coefficients acquired by Eq. (30) are about two times of those obtained by Carril, *et al.* (2003). The differences between the Reynolds numbers, turbulent flows of the two wind tunnel tests and the side ratios of the two lattice tower models are possible causes of the great diversities between the RMS along-wind and across-wind force coefficients of the two lattice tower models. Nevertheless, the ratios of the RMS along-wind force coefficients to RMS across-wind force coefficients of both the two models are in the range of 2.3 to 3.0.

Though the numerical models of 3-D generalized wind loads of three kinds of typical lattice towers in the frequency domain were experimentally obtained in this paper, extensive phenomena revealed by this investigation are noticeable, further probes into the mechanism and formation of 3-D dynamic wind loads, especially across-wind dynamic loads, on lattice towers are still needed. The characteristics of the spectral densities of the across-wind loads on a lattice tower are quite different from those of the along-wind loads, and also, they are quite different from the characteristics of the across-wind velocity spectra. Fig. 18 is the comparison of the along-wind and across-wind velocity spectra measured in the TJ-2 boundary layer wind tunnel, which agree with the von-Karman type spectrum and the across-wind velocity spectrum in ESDU(2001) well respectively. It indicates that the basic characteristics of the along-wind and across-wind velocity spectra are similar, although the magnitude of the along-wind velocity spectrum is much greater than that of across-wind velocity spectrum.

Actually, the dominant frequencies of the across-wind generalized force spectra are rather higher than those of the across-wind and along-wind velocity spectra; therefore it seems that the main

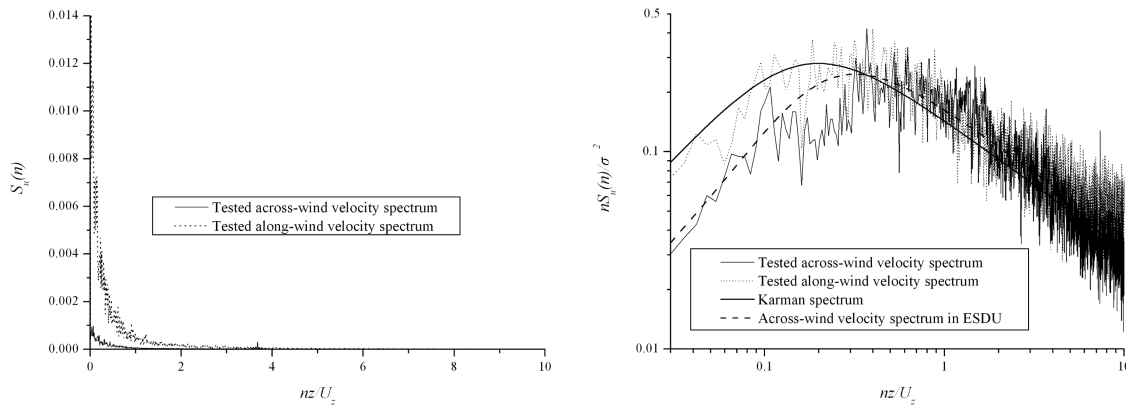


Fig. 18 The comparison of along-wind and across-wind velocity spectra measured in the TJ-2 boundary layer wind tunnel

contributor of across-wind dynamic loads on lattice towers is not across-wind or along-wind turbulence in the approaching flow. The spectral peaks of the across-wind generalized force are located between reduced frequency 0.1 and 0.2, and it should be attentively pointed out that the width B , in the expression of reduced frequency nB/V_H , is the width of the lattice tower, not the width of the structural member. When wind speed in the wind tunnel tests increases step by step, the spectral peak of the across-wind force versus frequency gently removes towards the right, but the spectral peak of the across-wind force versus reduced frequency is still located between reduced frequency 0.1 and 0.2. These phenomena suggest that although approaching flow can pass through a lattice tower, the interactions of numerous characteristic wakes of structural members may form an integral wake of the lattice tower, and the characteristic dimension of this integral wake is the width of the lattice tower, not the width of the structural members. This integral wake of lattice towers is probably the governing mechanism for the formation of the across-wind dynamic loads on lattice towers.

6. Conclusions

The main conclusions obtained by this investigation are as follows:

(1) The main cause of across-wind dynamic loads on lattice towers is probably the integral wake of lattice towers. The characteristics of spectral densities of across-wind loads on lattice towers are quite different from those of along-wind loads. The spectral density curves of the across-wind loads on lattice towers are thickly one-peak shaped, and the dominant frequencies of the across-wind generalized force spectra are rather higher than those of the along-wind generalized force spectra, and the peak of the across-wind generalized force spectrum is located between reduced frequency 0.1 and 0.2. In the meantime, the magnitudes of across-wind dynamic loads on lattice towers are much less than those of along-wind dynamic loads on lattice towers.

(2) The spectral densities of the generalized along-wind loads on lattice towers are provided with obvious characteristics of longitudinal wind turbulence. When the angle of the approaching flow is just between the X-axial and Y-axial directions, the spectral densities of the generalized X-axial and Y-axial wind loads become similar to each other, and their dominant characteristics appear to be those of longitudinal wind turbulence.

(3) The spectral density curves of generalized torsional wind loads on lattice towers have wide-

band characteristics with a spectral peak located at the very lowest reduced frequencies. The characteristics of the spectral densities of generalized torsional wind loads indicate that longitudinal wind turbulence is the main contributor of torsional wind loads on lattice towers. The magnitudes of generalized torsional wind loads on lattice towers are fairly small, especially those on the TV tower.

(4) The cross section shapes of the lattice members may considerably influence the magnitudes of the fluctuating 3-D wind loads on lattice towers, but do not greatly influence the characteristics of the spectral densities of the generalized 3-D wind loads on lattice towers. However, when the dimensions and cross sections of some local members of a lattice tower dramatically change, like on a TV tower, the spectral densities of the generalized 3-D wind loads on the tower will become partially irregular.

Acknowledgements

The research presented in this paper was supported by the China National Science Foundation under project No. 50278073, which is gratefully acknowledged.

References

- Glanville, M.J. and Kwok, K. C. S. (1995), "Dynamic characteristics and wind induced responses of a steel frame tower", *J. Wind Eng. Ind. Aerodyn.* 54-55, 133-149.
- Ballio, G., Meberini, F. and Solari, G. (1992), "A 60 year old 100m high steel tower: limit states under wind actions", *J. Wind Eng. Ind. Aerodyn.* 43(1-3), 2125.
- Holmes, J.D. (1994), "Along-wind responses of lattice tower: Part I-derivation of expressions for gust response factors", *Eng. Struct.*, 16(4), 287-292.
- Holmes, J.D. (1996), "Along-wind responses of lattice tower: Part II-aerodynamic damping and deflections", *Eng. Struct.*, 18(7), 483-488.
- Holmes, J.D. (1996), "Along-wind responses of lattice tower: Part III-effective load distributions", *Eng. Struct.*, 18(7), 489-494.
- Holmes, J.D., Schafer, B.L. and Banks, R.W. (1992), "Wind-induced vibration of a large broadcasting tower", *J. Wind Eng. Ind. Aerodyn.* 43(1-3), 2101-2109.
- Juhasova, E. (1997), "Quasi-static versus dynamic space wind response of slender structures", *J. Wind Eng. Ind. Aerodyn.*, 69-71, 757-766.
- Yasui, H. *et al.* (1999), "Analytic study on wind-induced vibration of power transmission towers", *J. Wind Eng. Ind. Aerodyn.*, 83(1-3), 431-441.
- Carril, C.F. and Isyumov, N. (2003), "Experimental study of the wind forces on rectangular latticed communication towers with antennas", *J. Wind Eng. Ind. Aerodyn.* 91(8), 1007-1022.
- Harikrishna, P., Shanmugasundaram, J., Gomathinayagam S. and Lakshmanan, N. (1999), "Analytical and experimental studies on the gust response of a 52m tall steel lattice tower under wind loading", *Comput. Struct.*, 70(2), 149-160.
- Savory, E., Parke, G.A.R., Zeinoddini, M., Toy, N. and Disney, P. (2001), "Modelling of tornado and microburst-induced wind loading and failure of a lattice transmission tower", *Eng. Struct.*, 23(4), 365-375.
- Venkateswarlu, B., Harikrishna, P., Rajan, S.S. and Kumar, M.S.R. (1994), "Stochastic gust response of microwave lattice towers", *Comput. Struct.*, 52(5), 1031-1041.
- Wyatt, T.A. (1992), "Dynamic gust response of inclined towers", *J. Wind Eng. Ind. Aerodyn.* 43(1-3), 2153-2163.
- Wang, D.H. and Liang, S.G. (2004), "The study of mechanical model of along-wind equivalent static loads on tall buildings", *Acta Mechanica Solida Sinica*, 25, S. Issue, 79-84(In Chinese).
- European Standard. (2004), Eurocod1: Actions on structures-general actions - Part 1-4: wind actions, Ref. No. prEN 1991-1-4.
- ASCE Standard. (2002), ASCE 7-02: Minimum Design Loads for Buildings and Other Structures. New York.
- ESDU (2001), Characteristics of atmospheric turbulence near the ground, Part II: Single point data for strong winds (neutral atmosphere), Wind engineering Sub-series, Data Item 85020, London.